Journal of Clinical and Cellular Immunology

OPEN ACCESS Freely available online

Research Article

# Imaging the Cytokine Receptor CXCR4 in Atherosclerotic Plaques with [$^{68}$Ga]-APD: A Novel Agent on Computer Simulation Approach

**Chien-Chung Hsia*, Chung-Hsin Yeh, Chun-Tang Chen, Cheng Liang Peng**

*Department of Isotope Application, Institute of Nuclear Energy Research, Taoyuan (ROC), Taiwan*

## ABSTRACT

**Introduction:** C-X-C motif chemokine receptor 4 (CXCR4) plays a prominent role in inflammation, atherosclerosis, and cancer biology. Therefore, CXCR4 represents a promising target for molecular imaging in cardiovascular diseases such as atherosclerosis and arterial wall injury.CXCR4 and its cognate ligand, stromal cell–derived factor 1α (SDF-1α), induced monocyte recruitment to the injured endothelium and subsequent plaque formation is the crucial progression of atherosclerosis. CXCR4 was been proved to be intensively expressed on monocytes/macrophage. [68Ga]-APD, based on CXCR4 antagonists TIQ-15, had designed as a PET tracer for imaging atherosclerosis. The aim of this study was to evaluate the biological characteristics of [68Ga]-APD, and compared with [18F]-FDG, [18F]-NaF, and [68Ga]-Pentixafor.

**Results:** The specification and quality of APD was identified by Mass, NMR and HPLC. After being labeled with Ga-68 under acetate buffer (pH=5.5), radiochemical purity was over 90% and stable for more than 4 hours in 37°C human serum. After being injected from tail vein on apolipoprotein-E-deficient (ApoE-/-) atherosclerotic mice, hydrophilic [68Ga]-APD was quickly eliminate from the kidney and bladder and accumulate in the atherosclerotic aorta. The highest target/background ratio (TBR) on atherosclerotic sites were 17.68 ± 0.71 (n=3) on high-fat diet ApoE-/- mice for 12 weeks after [68Ga]-APD injection about 1 hour. However, the TBR of [68Ga]-Pentixafor was only 2.06 ± 0.67 (n=3) on the same mice model. Competitive study represented that CXCR4 antagonist AMD3465 could effectively block the uptake of [68Ga]-APD on the atherosclerotic site and CXCR4 expression organs. Comparing with [18F]-FDG and [18F]-NaF, [68Ga]-APD represented relatively better TBR and specificity on the imaging of atherosclerotic lesions.

**Conclusion:** *In vivo* evaluation of CXCR4 expression in ApoE-/- mice revealed the high TBR of [68Ga]-APD on the atherosclerotic aorta and better than [68Ga]-Pentixafor. These evidences represented its feasible as a surrogate marker for inflammatory atherosclerosis.

**Keywords:** Autism spectrum disorders; Cytokine; Monocytes; microRNA (miRNA)

## INTRODUCTION

Although the diet management and medical improvement in treating Cardio Vascular Diseases (CVD), atherosclerotic plaque-induced stroke and Coronary Heart Disease (CHD), heart attack, or angina are one of the leading causes of mortality and morbidity worldwide [1,2]. The pathogenesis of atherosclerosis is characterized by the chronic accumulation of lipids and pro-inflammatory immune cells to the focal arterial wall and progressively narrows the lumen of the artery [3-5]. Owing to the unstable plaques by the pathologic mechanisms of inflammation, atherosclerotic plaque formation can be diagnosis from the mechanism of inflammation [6,7]. Within the inflammation and different aspects of the atherosclerotic plaque, activated macrophages play the most interesting target in the atherosclerotic lesion [8]. Imaging atherosclerosis with PET/CT characterizes atherosclerotic plaques on a molecular level and enables the quantification of arterial calcification [9]. Many Functional PET imaging tracers have been tried to targeting molecular elements of atherosclerosis of increasing the glucose metabolism by the inflammatory cells [10-13] and detect micro-calcifications around the arterial wall [14-16], such as [18F]-FDG and [18F]-NaF, respectively. The

**Correspondence to:** Chien-Chung Hsia, Department of Isotope Application, Institute of Nuclear Energy Research, Taoyuan, Taiwan (ROC), Tel: 886-3-4711400; Ext: 7159; E-mail: hsiacc@yahoo.com

**Received:** 06-Jun-2022, Manuscript No. JCCI-22-17763; **Editor assigned:** 09-Jun-2022, PreQC No. JCCI-22-17763 (PQ); **Reviewed:** 23-Jun-2022, QC No. JCCI-22-17763; **Revised:** 30-Jun-2022, Manuscript No. JCCI-22-17763 (R); **Published:** 07-Jul-2022, DOI: 10.35248/2155-9899.22.13.667

**Citation:** Hsia CC, Yeh CH, Chen CT, Peng CL (2022) Imaging the Cytokine Receptor CXCR4 in Atherosclerotic Plaques with [68Ga]-APD: A Novel Agent on Computer Simulation Approach. J Clin Cell Immunol.13:667.

7-transmembrane helix G-protein–coupled receptor, Chemokine C-X-C motif receptor 4 (CXCR4), and its cognate ligand, stromal cell-derived factor 1a (SDF-1a/CXCL12), induced monocyte recruitment to the injured endothelium and subsequent plaque formation is the crucial progression of atherosclerosis. CXCR4 is also been proven to be intensively expressed on monocytes/macrophage [17-21]. Recently, CXCR4-directed of macrophages PET imaging with [68Ga]-radiolabeled cyclic peptide, Pentixafor, has been provided to imaging neoplasms, hematologic, stroke, atherosclerosis, and myocardial infarction in humans by the mechanism of overexpression CXCR4 [22-25]. In addition, Tetra-azamacrocycles based small-molecule CXCR4 antagonists, such as AMD3100 and AMD3465, are also developed and proven to bind on human and mouse variants CXCR4 receptor. Jacobson et al., had developed a one-step radiosynthesis of [64Cu]-AMD3100 and exhibited a promising agent for visualization of CXCR4-positive tumors and metastases [26]. However, Copper (II) cyclam complexes are unlikely to have sufficient electrostatic/H-bonding between cyclam amine groups with aspartate residue side chains (171 and 262) and lead to high nonspecific hepatic accumulation to retain the metal ion *in vivo* [27].

The atherosclerotic-prone apolipoprotein E-deficient (ApoE-/-) mice were first developed in 1992 by homologous recombination of embryonic stem cells and currently use in the pre-clinical atherosclerotic model by down regulation of cholesterol transporter ATP-binding cassette subfamily A member 1 levels [28]. Poor lipoprotein clearance of atherosclerosis-prone apolipoprotein E-deficient (ApoE-/-) mice display the accumulation of cholesterol ester-enriched particles in the blood and promote the development of atherosclerotic plaques. ApoE-/- mice is well established for studying atherosclerotic lesions on aorta by high-fat chow diet or even a regular diet for several weeks. The atherosclerotic lesions in ApoE-/- mice resemble human lesions in their predilection sites and progression to the fibro-proliferative stage [29]. In this study, we investigate the biological characteristics of novel CXCR4 agent [68Ga]-APD, and compared with [18F]-FDG, [18F]-NaF, and [68Ga]-Pentixafor PET tracers on targeting atherosclerotic lesion by high fat diet ApoE-/- mice model.

## METHODOLOGY

### General

APD structure was designed and selected from Tetrahydroisoquinoline-Based CXCR4 Antagonist TIQ-15 by screening million's chemical fragments and evaluated its chemical binding energy on CXCR4 specific amino acids residue [30]. APD was synthesized at RDD LAB. INC, Taiwan and determined its specifications by NMR (JNM-ECZ500R/S1, JOEL USA, Inc), Mass (AB Sciex (Concord, ON, Canada) 4000QTRAP® mass spectrometry) and high-performance liquid chromatography (HPLC, Waters-2695, with UV and radio detector). Radio-thin-layer chromatography was performed on instant TLC chromatogram sheets (Sigma Chemical Company, USA), eluting with citrate buffer (pH=5.5) and Bioscan AR-2000 (Eckert and Ziegler, Germany). Pentixafor was purchased from UNION CHEMICAL IND. CO., LTD. Taiwan. [18F]-FDG and [18F]-NaF provided from Institute of Nuclear Energy Research, Taoyuan, Taiwan (Figure 1).

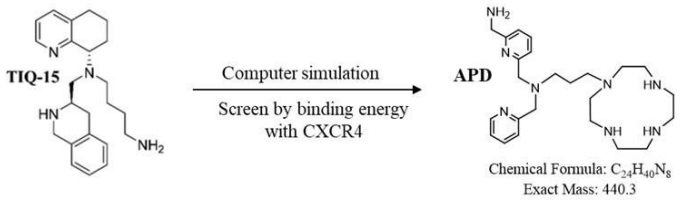


**Figure 1:** The structure of APD was designed from TIQ-15 by computer simulation and screen by binding energy with CXCR4.

### Preparation and radiochemical purity (RCP) analysis

APD (0.01~0.1 mg) dissolved in acetate buffer (pH 5.0~6.0) and then labeled with [68Ga]-GaCl3 (1~10mCi) for at least 20 minutes under 60~70℃.To determine the amount of impurity, the sample was chromatographed on ITLC-SG (Sigma Chemical Company, USA) using 0.1 M citrate buffer (pH 5.5) as the mobile phase (Rf=0: [68Ga]-APD, Rf=1: [68Ga]-GaCl3). [68Ga]-colloid was also determined by TLC with 1.25 M NH4Ac, pH 5.5: DMF (1:1) as a mobile phase (Rf=0: [68Ga]-colloid, Rf=1: [68Ga]-APD) [31].

A Waters system pump (Germering, D) and radiometric detection (Bioscan, Washington DC), were used for RP-HPLC analysis. C-18 column (Waters 5 μm, 80 Å, 250 × 4.6 mm). Flow rates of 0.8 mL/min were employed as the following: A linear gradient eluent starting from 30% A (0.1% TFA in water) and 70% B (0.1% TFA in acetonitrile), increasing to 90% B for 10 min, remaining constant at 90% B for another 15-30 min. The RCP was calculated expressing the peak corresponding to [68Ga]-APD as percentage of the total activity in the radio-chromatogram. The injected activity on the HPLC-column was in the order of 5 MBq. RCP of [68Ga]-Pentixafor was also determined by HPLC followed as previously described [33].

### Study product compliance

Compliance was calculated based on dispensed and returned study products. In the case of missing products or no return, compliance was estimated from subject diaries.

### Partition coefficient (n-Octanol/PBS) determination

To determine the hydrophilicity of [68Ga] -APD, the octanol/water partition coefficients (log P) were measured. Briefly, [68Ga]-APD (7.4 MBq) with phosphate-buffered saline (PBS, 5.0 mL, 0.15 M, pH 7.4) and n-octanol (5 mL) within a test tube. After vortexing for 1 min, tube was placed on bench for 3 min in room temperature. Samples (from each phase, 100 μL) were counted its radioactivity by using gamma-counter. The tests were reported as mean ± SD (n ≧ 3), independently.

### Mice and PET/CT acquisition

ApoE-/- mice experimental protocol had been approved by the Institutional Animal Care and Use Committee (IACUC) in the Institute of Nuclear Energy Research (Taoyuan, Taiwan) and followed the ARRIVE guidelines and the USPHS Policy on Human Care and Use of Laboratory Animals. Female ApoE-/- mice (provided from Taiwan University Hospital) (aged >8 weeks) housed in a controlled environment (22 ± 2°C and 50 ± 5% relative humidity) with a 12-h light-and-dark cycle and received a high-fat diet for accelerating atherosclerotic lesions. PET/CT imaging was performed on a Bioscan scanner (matrix size, 128 × 128 × 159; CT attenuation-corrected; non-scatter corrected) (Washington DC, USA) following a intravenous tail vein injection of approximately

14.8 MBq (0.4 mCi) of [68Ga] -APD into ApoE-/- mice (3-5 mice per group). Dynamic scans were acquired in list mode format for at least 120 min, and sorted into 22 frames, 0.5-mm sinogram bins for image reconstruction (4 × 15 s, 4 × 60 s, 11 × 300 s, 3 × 600 s). Mice were anesthetized with isoflurane (3% for induction and 2% for maintenance) throughout the experiment.

ApoE-/- mice was imaged with [68Ga]-APD (11.1 MBq) on 2, 8 and 12 weeks of high-fat diet to characterize different severity on atherosclerotic lesions. For competitive inhibition assay on [68Ga]-APD, a CXCR4 inhibitor AMD3465 (25 mg/kg) was injected before administration of 11.1 MBq of [68Ga]-APD on high-fat diet ApoE-/- mice for 12 weeks. [68Ga]- Pentixafor (11.1 MBq) was also administrated on the same mice model for comparing the efficacy on atherosclerotic lesions with [68Ga]-APD. [18F]- FDG PET/CT imaging was been performed after 6 h fasting period to ensure serum glucose levels below 130 mg/dL. To estimate the radioactivity concentration, volumes of interests had defined on coregistered PET/CT images using PMOD software. Target/Background Ratio (TBR) had calculated by placing a circular 2-mm volume of all interest organs/tissues around a site. TBRs were been calculated as focal uptake divided by blood pool.

### Autoradiographic studies on atherosclerosis

To visualize the distribution of [68Ga]-APD around the heart region, autoradiography was performed using 20-μm-thick fresh-frozen heart and aorta sections derived from ApoE-/- mice. The specimens were exposed to phosphor imaging plates (MS-2040, Fuji Photo Film Co. Ltd.) for 2 h in the [68Ga]-APD examination. Subsequently, the radioactivity distributions were imaged by using imaging analyzer BAS 4000 (Fuji Photo Film Co. Ltd.).

### Statistical analysis

The statistical significance of comparisons of radioactivity in organs in PET studies was based on 2-sided, 2-sample Student t-tests. For all tests, $P<0.05$ was considered statistically significance and represented on figures. Results were reported as mean ± SD (n ≧ 3).

## RESULTS

### Synthesis and characterization

The novel CXCR4 antagonist structure of APD was represented (Figure 1). The binding energy of APD and TIQ-15 were -300.3 kcal/mol and -80.4 kJ/mol, respectively. Chemical characterization of APD had verified by NMR, mass spectrum and HPLC. 1H NMR (D2O) δ8.46-8.45 (m, 1 H), 7.84-7.80 (m, 2.H), 7.49-7.47 (d, 1H), 7.41-7.34(m, 3H), 3.70-3.90 (m, 6H),2.78-2.47 (m, 20H), 1.73-1.67 (m, 2H). 13C NMR (D2O) δ160.30, 157.53, 148.16, 138.61, 137.96, 124.63, 123.08, 122.84, 120.45, 59.98, 53.29, 50.30, 45.93, 45.10, 43.92, 43.29, 23.31. The molecular weight and purity of APD was measured as [M+H]+=441.51 and over 98%, respectively.

### Radiochemical purity (RCP) and partition coefficient (n-Octanol/PBS) determination

After the labeled of APD with [68Ga]-GaCl3 under 60~70℃ for 20 minutes, radiochemical purity of [68Ga]-APD was calculated by paper chromatography on SG-ITLC strip with citrate buffer (pH 5.5) (Figure 2A). The chromatogram represented that the radiochemical purity of [68Ga]-APD was over 90%. [68Ga]-colloid was excluded as the impurity by the determination of TLC with 1.25 M NH4Ac, pH 5.5: DMF (1:1) as a mobile phase.

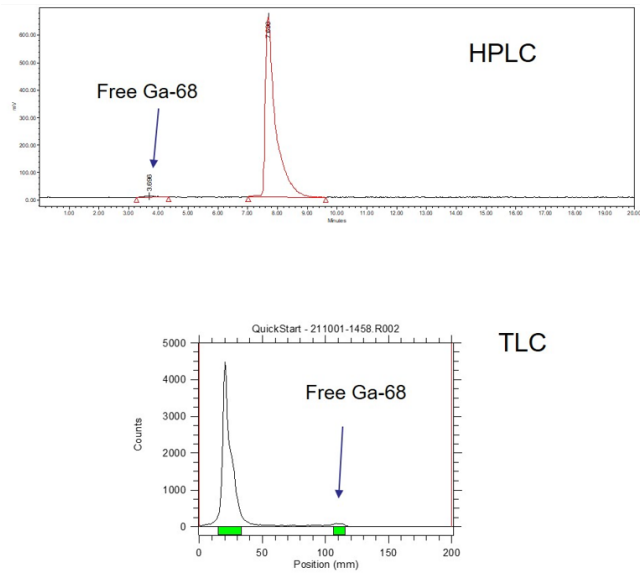


**Figure 2:** Radiochemical purity of [68Ga]-APD was determined by HPLC (up) and TLC (down). HPLC and TLC could separate the impurity and prove the radiochemical purity >90%.

### PET/CT studies on ApoE-/- atherosclerotic model mice

In the competitive inhibition study, the PET/CT images represented that [68Ga]-APD could be apparently blocked the uptake on atherosclerotic lesion by pre-injection of a dose (5 mg/kg) of CXCR4 inhibitor AMD3465 on high fat diet ApoE-/- mice for 12 weeks. Furthermore, the pre-dosing with AMD-3465 could also significantly reduce the TBR of [68Ga]-APD at CXCR4-overexpression organs, such as liver, lung, and kidney (27). These evidences provided that [68Ga]-APD was specific binding on CXCR4 ($P<0.05$) (Figure 3).

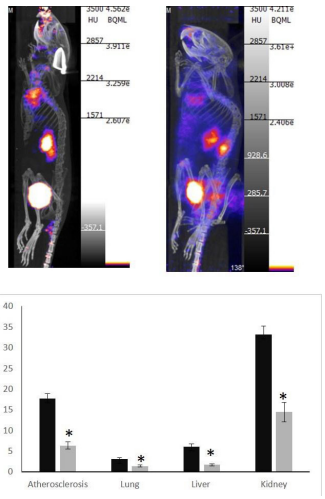


**Figure 3:** Biodistribution of [68Ga]-APD on a high-fat diet for 12 weeks. [68Ga]-APD was excreted quickly from the kidney and the TBR of atherosclerotic site was 17.68 ± 0.71 after i.v. injection for 0.5 h. CXCR4 antagonist AMD3465 could inhibit the uptake on the CXCR4-atherosclerotic site, lung, liver and kidney ($P<0.05$). **Note:** (■) [68ga]-APD; (■) [68Ga]-APD+AMD3465.

In comparing the PET images of [68Ga]-APD (11.1 MBq) on the different duration ApoE-/- mice, the TBR was 7.52 ± 0.83, 9.65 ± 0.69 and 17.68 ± 0.71 on 2, 8 and 12 weeks of high fat diet, respectively. The TBR of [68Ga]-APD was decreased with time (n=3) (Figure 4).

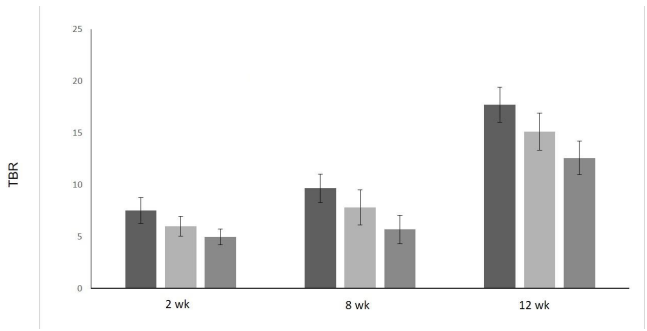


**Figure 4:** TBR of [68Ga]-APD on ApoE-/- mice for a high-fat diet 2, 8 and 12 weeks. The TBR was increasing with high-fat diet time (n=3). **Note:** (■) 1h; (■) 2h; (■) 3h.

Kidney and bladder had higher tracer uptake, providing that [68Ga]-APD might primarily excrete from the kidney to bladder. For comparing the imaging efficacy on atherosclerotic aorta between [68Ga]-APD and [68Ga]-Pentixafor (RCP>95%) on high-fat diet ApoE-/- mice for 12 weeks, the results represented that TBR of [68Ga]-APD was better than [68Ga]-Pentixafor during the imaging time (Figure 5).

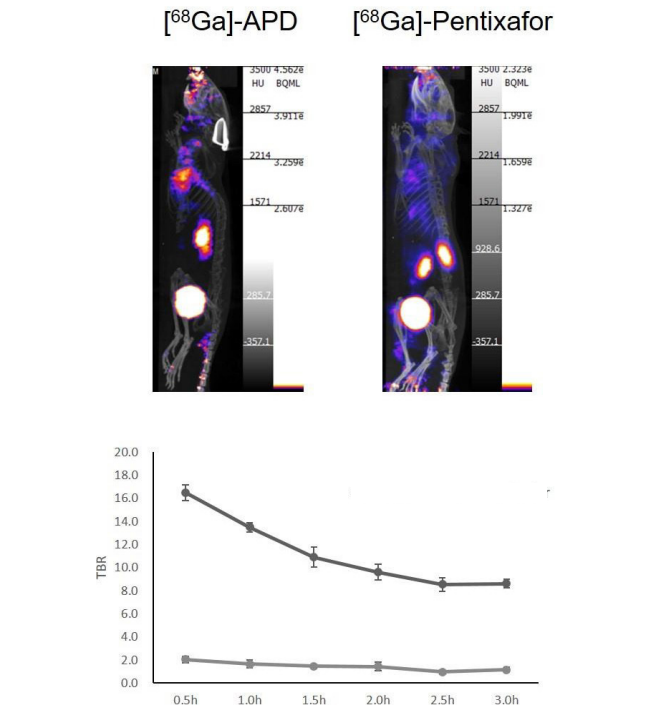


**Figure 5:** TBR of [68Ga]-APD and [68Ga]-Pentixafor on ApoE-/- mice for a high- fat diet for 12 weeks. The TBR of [68Ga]-APD was 2.06 ± 0.67 at 0.5 h after injection and decreased with time. However, the TBR of [68Ga]-APD was about 8 times higher than [68Ga]-Pentixafor (P<0.05). **Note:** (—●—) APD; (—●—) Pentixafor.

The TBR on [68Ga]-Pentixafor was approximately matched as previously described [22-25]. [18F]-FDG injection was been performed after fasting for at least 6 h to ensure serum glucose levels below 130 mg/dL. The PET image represents that [18F]-FDG accumulated mainly on the myocardium. However, the highest TBR of [18F]-FDG was only 1.53 ± 0.75 (n=3) on the atherosclerotic aorta (ApoE-/- mice, high-fat diet 10 weeks). Furthermore, [18F]-NaF could not effectively target atherosclerotic site by the reason of lacking calcified lesions on this model (ApoE-/- mice, high-fat diet 10 weeks) (Figure 6).

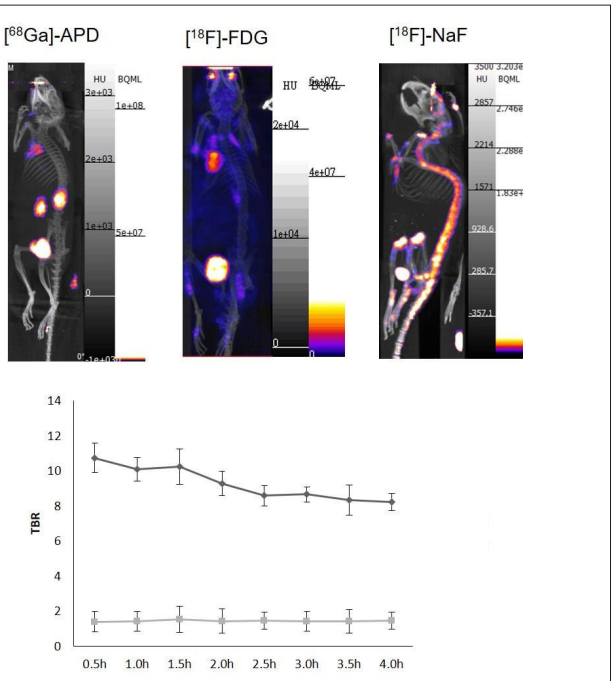


**Figure 6:** TBR of [68Ga]-APD, [18F]-FDG and [18F]-NaF on ApoE-/- mice high fat diet for 10 weeks. [18F]-FDG was major distributed in the myocardium. [68Ga]-APD distributed specifically in the atherosclerotic site. [18F]-NaF could not find to target on heart and atherosclerotic site. **Note:** (—●—) APD; (—■—) FDG.

## Autoradiographic studies on atherosclerosis

From the PET/CT image of [68Ga]-APD in Figure 6, there was tracer specific targeting in the chest region. For verified the distribution of [68Ga]-APD, the slide autoradiogram of [68Ga]-APD had shown obvious high radioactivity accumulating in the aorta region but not on the heart. Oil Red O stained tissues had also proved the distribution of lipids on the atherosclerotic aorta (Figure 7).

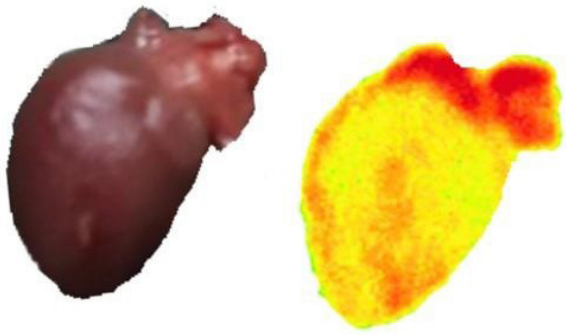

**Figure 7:** Tissue slide autoradiogram of [68Ga]-APD had shown obvious high radioactivity accumulating in the aorta region but not on the heart.

# DISCUSSION

This study reports a novel CXCR4 antagonist structure APD was been designed by replacing over million's chemical fragments on the structure of TIQ-15 and evaluating its binding energy. After being labeled with Ga-68, [68Ga]-APD represent good sensitivity and specificity to CXCR4 expression atherosclerotic lesions.

Atherosclerotic plaque formation, development, and progression are complex and involve many factors, including endothelial dysfunction, elevated cholesterol and immune activity. As plaques

in the arterial walls build and progress, the rupture on the arteries may be occluded distally and block blood flow into heart muscle, brain, and other parts of the body [1]. Inflammation is an important component of atherosclerotic plaque vulnerability. Owing to the glucose uptake in active and lipid-rich macrophages on inflammatory plaques, it is likely to use [18F]-FDG as a marker to detect small lesions of atherosclerotic plaques. However, [18F]-FDG plaque imaging is limited by non-specificity on atherosclerotic lesions. In addition, the constant motion of cardiac cycle and the significant uptake of [18F]-FDG in the myocardium has decreased the enthusiasm to use this tracer in atherosclerotic imaging [25]. [18F]-NaF have significant advantages in the assessment of atherosclerotic plaques imaging with regards to its more accurately and precisely in detecting and characterizing plaques than [18F]-FDG. Therefore, the future of PET imaging to assess atherosclerosis will predict to heavily rely on [18F]-NaF [34].

Oxidized low-density lipoprotein (Ox-LDL) and vascular hypoxic process might significantly induce macrophage to overexpression CXCR4 and enhanced the atherosclerotic progression. In comparison within early or advanced atherosclerotic lesions, Bot et al. had found that CXCR4 expression was significantly pronounced in advanced unstable lesions [35]. Remarkably, the expression of CXCR4 protein was co-localized with macrophage expression in inflamed vulnerable plaque lesions. This finding might support the concept that CXCR4 played a recruitment role for leukocytes into the vessel wall and could serve as a good biomarker for atherosclerotic imaging [27].

There are many PET tracers have tried to image atherosclerotic changes based on the macrophage to expression CXCR4. [68Ga]-Pentixafor is one of the successful CXCR4 clinical trial tracers to image atherosclerosis with a clear view of vascular uptake and a relatively clear background. Li et al. had shown that patients with higher uptake of [68Ga]-Pentixafor represented a higher incidence of metabolic syndrome and might suggest its clinical potential in the evaluation of diseased vessels [36]. Derlin et al. had also shown that accumulation of [68Ga]-Pentixafor and [18F]-FDG represented only a weak correlation by observed in non-calcified lesions [37].

Tetrahydroisoquinoline-Based CXCR4 antagonists TIQ-15 had been found to have good oral bioavailability and its active structure was confirmed to interaction with ASP 97, Tyr116 and Glu288 residue on CXCR4 [38]. In this study, a novel CXCR4 tracer APD was been designed from the structure of TIQ-15 to become a tracer for imaging atherosclerosis. The selected structure of APD was been screened by replacing over million's chemical fragments on the structure of TIQ-15 and evaluating its docking efficacy by binding energy. In our preliminary study, the cellular uptake of [68Ga]-APD could be blocked by using CXCR4 antagonist AMD3465 on CXCR4-expression HT-29 colon cells. The PET image of [68Ga]-APD on ApoE-/- atherosclerotic model had shown high selective uptake on atherosclerotic aorta. Owing to the good hydrophilicity (Log P=-1.4), [68Ga]-APD PET image showed a quick excretion from kidney and with a relatively low background. CXCR4 antagonist AMD3465 (5 mg/kg) could effectively reduce the uptake on atherosclerotic plaque, liver, lung and kidney at 60 min before tracer administration which suggested its specific binding on CXCR4 in Figure 3. Human serum stability assays also showed that [68Ga]-APD could be stable for over 4 h under 37°C human serum. For confirming the distribution of isotope labeled APD on the atherosclerotic aorta, tissue frozen section had also been done after the bio-distributed of [68Ga]-APD (RCP>90%) for 30 mins on ApoE-/- mice. The autoradiogram represented that [68Ga]-APD was distributed on atherosclerotic aorta which can be seen in Figure 7. Atherosclerotic plaques may stabilize or reduce in size, lipid content, foam cell content, and macrophage inflammation through Macrophage Reverse Cholesterol Transport (RCT) mechanism by eliminating oxidized low-density lipoprotein (Ox-LDL) from atherosclerotic plaques. [39,40]. Early detection and therapy is the key to improving the atherosclerotic prognosis at present. In this study, [68Ga]-APD PET image provides the possibility in the early diagnosis of atherosclerosis with high sensitivity and specificity than [68Ga]-Pentixafor.

## CONCLUSION

*In vivo* evaluation of CXCR4 expression in ApoE-/- mice revealed the high TBR of [68Ga]-APD on the atherosclerotic aorta and better than [68Ga]-Pentixafor. These evidences represented its feasible as a surrogate marker for inflammatory atherosclerosis.

## AUTHORS CONTRIBUTIONS

CH conducted experiments and wrote the manuscript. CY, CC and CP reviewed the study design and helped to cultured cells, raised mice and conducted mice's experiments. All authors read and approved the final manuscript.

## ACKNOWLEDGEMENTS

I would like to express my deep and sincere gratitude to research colleagues, Dr. Mei-Hui Wang, Dr. Hung-Wen Yu, Dr. Ying-Hsia Shih and all of the team members for his genuine support throughout this research work. I thank the management of Institute of Nuclear Energy Research for their financial support to do this work. I also thank the directors Dr. Shiou-Shiow Farn, Dr. Jeng-Hung Lee and Dr. Jeng-Jong Wang and Dr. Chih-Hsien Chang for their genuine support to complete this thesis successfully. Finally, my thanks go to all the people who have supported me to complete the research work directly or indirectly.

## DECLARATIONS

### Ethics approval and consent to participate

ApoE-/- mice experimental protocol had approved by the Institutional Animal Care and Use Committee (IACUC) in the Institute of Nuclear Energy Research (Taoyuan, Taiwan) and followed the ARRIVE guidelines and the USPHS Policy on Human Care and Use of Laboratory Animals. ApoE-/- mice had gotten the consent to provide from Taiwan University Hospital.

## CONSENT FOR PUBLICATION

Not applicable.

## AVAILABILITY OF DATA AND MATERIAL

All the raw data of this study, including PET images and data can be obtained through the corresponding authors on reasonable request.

## COMPETING INTERESTS

The authors declare that no other potential conflict of interest relevant to this article exists.

## COMPETING INTERESTS

The authors declare that no other

## FUNDING

Funding was all provided by Institute of Nuclear Energy Research, Taiwan.

## REFERENCES

1. MMunger E, Hickey JW, Dey AK, Jafri MS, Kinser JM, Mehta NN. Application of machine learning in understanding atherosclerosis: Emerging insights. APL bioengineering. 2021;5(1):011505.
2. Nakahara T, Strauss HW. From inflammation to calcification in atherosclerosis. Eur J Nucl Med Mol Imaging. 2017;44(5):858-60.
3. Bild DE, Bluemke DA, Burke GL, Detrano R, Diez Roux AV, Folsom AR,et al. Multi-ethnic study of atherosclerosis: objectives and design. Am J Epidemiol. 2002;156(9):871-81.
4. Cooper CJ, Murphy TP, Cutlip DE, Jamerson K, Henrich W, Reid DM, et al. Stenting and medical therapy for atherosclerotic renal-artery stenosis. N Engl J Med. 2014;370(1):13-22.
5. Chen T, Brewster P, Tuttle KR, Dworkin LD, Henrich W, Greco BA, et al. Prediction of cardiovascular outcomes with machine learning techniques: application to the cardiovascular outcomes in renal atherosclerotic lesions (CORAL) study. Int J Nephrol Renovasc Dis. 2019;12:49.
6. Libby P. Inflammation in atherosclerosis. Arteriosclerosis, thrombosis, and vascular biology. 2012 ;32(9):2045-51.
7. Silvestre-Roig C, De Winther MP, Weber C, Daemen MJ, Lutgens E, Soehnlein O. Atherosclerotic plaque destabilization: mechanisms, models, and therapeutic strategies. Circ Res. 2014;114(1):214-26.
8. Moore KJ, Sheedy FJ, Fisher EA. Macrophages in atherosclerosis: A dynamic balance. Nat Rev Immunol. 2013;13(10):709-21.
9. Joseph P, Tawakol A. Imaging atherosclerosis with positron emission tomography. Eur Heart J. 2016;37(39):2974-80.
10. Tarkin JM, Joshi FR, Evans NR, Chowdhury MM, Figg NL, Shah AV, et al. Detection of atherosclerotic inflammation by 68Ga-DOTATATE PET compared to [18F] FDG PET imaging. J Am Coll Cardiol. 2017;69(14):1774-91.
11. Pauwels EK, Sturm EJ, Bombardieri E, Cleton FJ, Stokkel MP. Positron-emission tomography with [18F] fluorodeoxyglucose. J Cancer Res Clin Oncol. 2000;126(10):549-59.
12. Hetterich H, Rominger A, Walter L, Habs M, Volpers S, Hacker M, et al. Natural history of atherosclerotic disease progression as assessed by 18F-FDG PET/CT. Int J Cardiovasc Imaging. 2016; 32(1):49-59.
13. Rudd JH, Myers KS, Bansilal S, Machac J, Pinto CA, Tong C, et al. Atherosclerosis inflammation imaging with 18F-FDG PET: carotid, iliac, and femoral uptake reproducibility, quantification methods, and recommendations. J Nucl Med. 2008;49(6):871-8.
14. Derlin T, Richter U, Bannas P, Begemann P, Buchert R, Mester J, et al. Feasibility of 18F-sodium fluoride PET/CT for imaging of atherosclerotic plaque. J Nucl Med. 2010;51(6):862-5.
15. Derlin T, Wisotzki C, Richter U, Apostolova I, Bannas P, Weber C, et al. In vivo imaging of mineral deposition in carotid plaque using 18F-sodium fluoride PET/CT: correlation with atherogenic risk factors. J Nucl Med. 2011;52(3):362-8.
16. Fiz F, Morbelli S, Piccardo A, Bauckneht M, Ferrarazzo G, Pestarino E, et al. 18F-NaF uptake by atherosclerotic plaque on PET/CT imaging: Inverse correlation between calcification density and mineral metabolic activity. J Nucl Med. 2015;56(7):1019-23.
17. Zernecke A, Bot I, Djalali-Talab Y, Shagdarsuren E, Bidzhekov K, Meiler S, et al. Protective role of CXC receptor 4/CXC ligand 12 unveils the importance of neutrophils in atherosclerosis. Circ Res. 2008;102(2):209-17.
18. Döring Y, Noels H, Van Der Vorst EP, Neideck C, Egea V, Drechsler M, et al. Vascular CXCR4 limits atherosclerosis by maintaining arterial integrity: Evidence from mouse and human studies. Circulation. 2017;136(4):388-403.
19. Döring Y, van der Vorst EP, Duchene J, Jansen Y, Gencer S, Bidzhekov K, et al. CXCL12 derived from endothelial cells promotes atherosclerosis to drive coronary artery disease. Circulation.2019;139(10):1338-40.
20. Merckelbach S, van der Vorst EP, Kallmayer M, Rischpler C, Burgkart R, Döring Y, et al. Expression and cellular localization of CXCR4 and CXCL12 in human carotid atherosclerotic plaques. Thromb Haemost. 2018;118(01):195-206.
21. Demmer O, Gourni E, Schumacher U, Kessler H, Wester HJ. PET imaging of CXCR4 receptors in cancer by a new optimized ligand. ChemMedChem. 2011 Oct 4;6(10):1789-91.
22. Hyafil F, Pelisek J, Laitinen I, Schottelius M, Mohring M, Döring Y, et al. Imaging the cytokine receptor CXCR4 in atherosclerotic plaques with the radiotracer 68Ga-pentixafor for PET. J Nucl Med. 2017;58(3):499-506.
23. Weiberg D, Thackeray JT, Daum G, Sohns JM, Kropf S, Wester HJ, et al. Clinical molecular imaging of chemokine receptor CXCR4 expression in atherosclerotic plaque using 68Ga-pentixafor PET: Correlation with cardiovascular risk factors and calcified plaque burden. J Nucl Med. 2018;59(2):266-72.
24. Derlin T, Sedding DG, Dutzmann J, Haghikia A, König T, Napp LC, et al. Imaging of chemokine receptor CXCR4 expression in culprit and nonculprit coronary atherosclerotic plaque using motion-corrected [68Ga] pentixafor PET/CT. Eur J Nucl Med Mol Imaging. 2018;45(11):1934-44.
25. Lapa C, Schreder M, Schirbel A, Samnick S, Kortüm KM, Herrmann K, et al. [68Ga] Pentixafor-PET/CT for imaging of chemokine receptor CXCR4 expression in multiple myeloma-Comparison to [18F] FDG and laboratory values. Theranostics. 2017;7(1):205.
26. Jacobson O, Weiss ID, Szajek L, Farber JM, Kiesewetter DO. 64Cu-AMD3100—a novel imaging agent for targeting chemokine receptor CXCR4. Bioorg Med Chem. 2009;17(4):1486-93.
27. Hsia CC, Yeh CH, Chen CT, Peng CL. Imaging the cytokine receptor CXCR4 in atherosclerotic plaques with [68Ga]-APD: A novel radiotracer on computer simulation approach.
28. Lo Sasso G, Schlage WK, Boué S, Veljkovic E, Peitsch MC, Hoeng J. The Apoe−/− mouse model: A suitable model to study cardiovascular and respiratory diseases in the context of cigarette smoke exposure and harm reduction. J Transl Med. 2016;14(1):1-6.
29. Wei L, Petryk J, Gaudet C, Kamkar M, Gan W, Duan Y, et al. Development of an inflammation imaging tracer, 111In-DOTA-DAPTA, targeting chemokine receptor CCR5 and preliminary evaluation in an ApoE−/− atherosclerosis mouse model. J Nucl Cardiol. 2019;26(4):1169-78.
30. Truax VM, Zhao H, Katzman BM, Prosser AR, Alcaraz AA, Saindane MT, et al. Discovery of tetrahydroisoquinoline-based CXCR4 antagonists. ACS Med Chem Lett. 2013;4(11):1025-30.
31. Brom M, Franssen GM, Joosten L, Gotthardt M, Boerman OC. The effect of purification of Ga-68-labeled exendin on in vivo distribution. EJNMMI Res. 2016;6(1):1-8.
32. Demmer O, Dijkgraaf I, Schumacher U, Marinelli L, Cosconati S, Gourni E, et al. Design, synthesis, and functionalization of dimeric peptides targeting chemokine receptor CXCR4. J Med Chem. 2011;54(21):7648-62.

33. Poschenrieder A, Schottelius M, Schwaiger M, Wester HJ. Preclinical evaluation of [68 Ga] NOTA-pentixafor for PET imaging of CXCR4 expression in vivo—a comparison to [68 Ga] pentixafor. EJNMMI Res. 2016 ;6(1):1-5.

34. Høilund-Carlsen PF, Sturek M, Alavi A, Gerke O. Atherosclerosis imaging with 18F-sodium fluoride PET: State-of-the-art review. Eur J Nucl Med Mol Imaging. 2020;47(6):1538-51.

35. Bot I, Daissormont IT, Zernecke A, van Puijvelde GH, Kramp B, de Jager SC, et al. CXCR4 blockade induces atherosclerosis by affecting neutrophil function. 2014;74:44-52.

36. Li X, Yu W, Wollenweber T, Lu X, Wei Y, Beitzke D, et al. [68Ga] Pentixafor PET/MR imaging of chemokine receptor 4 expression in the human carotid artery. Eur J Nucl Med Mol Imaging. 2019;46(8):1616-25.

37. Derlin T, Jonigk D, Bauersachs J, Bengel FM. Molecular Imaging of Chemokine Receptor CXCR4 in Non-Small Cell Lung Cancer Using 68Ga-Pentixafor PET/CT: Comparison With 18F-FDG. Clin Nucl Med. 2016;41(4):e204-5.

38. Miller EJ, Jecs E, Truax VM, Katzman BM, Tahirovic YA, Wilson RJ, et al. Discovery of tetrahydroisoquinoline-containing CXCR4 antagonists with improved in vitro ADMET properties. J Med Chem. 2018;61(3):946-79.

39. Ouimet M, Barrett TJ, Fisher EA. HDL and reverse cholesterol transport: Basic mechanisms and their roles in vascular health and disease. Circulation research. 2019;124(10):1505-18.

40. Heo GS, Sultan D, Liu Y. Current and novel radiopharmaceuticals for imaging cardiovascular inflammation. Q J Nucl Med Mol Imaging. 2020;64(1):4.